Chemical Engineering Journal 294 (2016) 254–263

Contents lists available at ScienceDirect

Chemical Engineering Journal

journal homepage: www.elsevier.com/locate/cej

High hydrothermal stability of Cu–SAPO-34 catalysts for the NH_3-SCR of NO*x*

Can Niu, Xiaoyan Shi, Fudong Liu [1], Kuo Liu, Lijuan Xie, Yan You *, Hong He *

State Key Joint Laboratory of Environment Simulation and Pollution Control, Research Center for Eco-environmental Sciences, Chinese Academy of Sciences, Beijing 100085, China

HIGHLIGHTS

- Relatively high calcination temperature was favorable for the deNO*x* catalytic activity of Cu–SAPO-34.
- Hydrothermal treatment increased NH_3-SCR activity due to the migration of CuO to isolated Cu^{2+} as well as the decreased activation barrier.
- High hydrothermal stability depend on the maintenance of acitive Cu^{2+}, crystallinity and the acidity after harsh treatment.

GRAPHICAL ABSTRACT

Cu–SAPO-34 catalysts prepared by the one-pot hydrothermal synthesis method showed high activity and outstanding hydrothermal stability due to the maintenance of isolated Cu^{2+}, the crystallinity and acidity as well as low activation barrier.

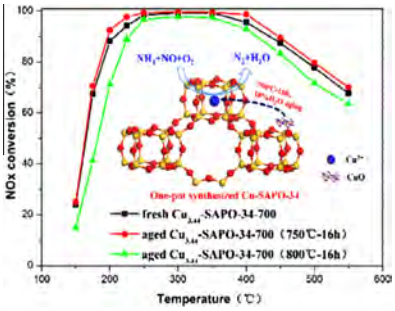

ARTICLE INFO

Article history:
Received 13 October 2015
Received in revised form 5 February 2016
Accepted 19 February 2016
Available online 27 February 2016

Keywords:
Cu–SAPO-34
NH_3-SCR
Hydrothermal stability
Copper species

ABSTRACT

The effects of calcination temperature, Cu source and co-template contents on the activity and hydrothermal stability of Cu–SAPO-34 catalysts prepared by the one-pot hydrothermal synthesis method were investigated. Appropriate calcination temperature was important for the deNO*x* activity of Cu–SAPO-34 catalyst. The amount of Cu source and co-template in the resulting gel could impact the Cu loading and the crystallization of the final Cu–SAPO-34. Preferably, hydrothermal treatment of the Cu–SAPO-34 catalyst with Cu loading ca. 3.44% at 750 °C for 16 h increased the NH_3-SCR activity slightly due to migration of CuO to isolated Cu^{2+} and the maintenance of the crystallinity as well as the acidity. Moreover, the catalyst aged at 800 °C for 16 h maintained >90% NO*x* conversion from 225 to 400 °C, and the crystallinity, active Cu^{2+} species and acidity in Cu–SAPO-34 were not destroyed completely after such harsh treatment. Meanwhile, kinetic analysis over fresh and aged Cu–SAPO-34 samples were conducted and the conclusion were in agreement with the NH_3-SCR tests, H_2-TPR and NH_3-TPD results.

1. Introduction

Pollutants, especially NO*x* from diesel engine exhaust, are the main sources of acid rain, haze and photochemical smog. Reducing NO*x* emissions is important for the improvement of air quality. The selective catalytic reduction of NO*x* by NH_3 (NH_3-SCR) is one of the most promising technologies for NO*x* emission control for diesel

* Corresponding authors at: State Key Joint Laboratory of Environment Simulation and Pollution Control, Research Center for Eco-environmental Sciences, Chinese Academy of Sciences, 18 ShuangQing Road, Haidian District, Beijing 100085, China. Tel./fax: +86 10 62849123.

E-mail addresses: yanyou@rcees.ac.cn (Y. You), honghe@rcees.ac.cn (H. He).

[1] Present address: Materials Sciences Division, Lawrence Berkeley National Laboratory, 1 Cyclotron Road, Berkeley, CA 94720, United States.

http://dx.doi.org/10.1016/j.cej.2016.02.086
1385-8947/

engines [1]. Due to the unstable operating conditions of diesel engines and periodically increasing the exhaust temperature to replicate diesel particulate filter (DPF) regeneration, excellent catalysts should meet the following essential requirements: good SCR activity over a wide operating temperature window, high selectivity for N_2, and outstanding hydrothermal stability.

Copper-based zeolites have been suggested as efficient catalysts for the NH_3-SCR reaction [2–5], and Cu–ZSM-5 was proposed to be the most promising [6,7]. However, the structure of the Cu–ZSM-5 catalyst collapsed easily after high temperature hydrothermal aging, leading to a conspicuous decline in NH_3-SCR activity [8]. Recently, Cu-CHA catalysts, (Cu supported on microporous zeolites (~0.38 nm pore size)), such as Cu–SSZ-13 and Cu–SAPO-34, have attracted much attention due to their higher NH_3-SCR activity and better hydrothermal stability compared to large or mesopore Cu-based zeolite catalysts [9,10].

Generally, Cu-CHA catalysts are prepared by ion-exchange methods (including aqueous solution and solid-state ion-exchange). The aqueous solution ion exchange method involves a two-step exchange process, filtering, washing and calcining, greatly limiting its application [11,12]. The solid-state ion exchange (SSIE) method is carried out under rather harsh conditions (calcining at 800 °C), leading to decomposition of the framework [13,14]. Recently, one-pot hydrothermal synthesis method used low-cost copper-tetraethylenepentamine (Cu-TEPA) as Cu source and template to prepare Cu-CHA directly which was much simpler to perform, and might be applicable at industrial scale [15]. Xie et al. [16] reported that the NO*x* conversion of one-pot synthesized $Cu_{3.8}$–SSZ-13 reached ca. 85% at 200 °C and maintained a level above 90% until 550 °C. Raquel et al. [17,18] reported that the NO conversion of $Cu_{3.3}$–SAPO-34 sample maintained a level above 90% between 200 and 450 °C and the NO conversion decreased about 10% over the whole temperature range after hydrothermal aging at 750 °C for 13 h. However, it is still a blank to investigate the one-pot hydrothermal synthesized Cu–SAPO-34 catalysts under more severe hydrothermal deactivation conditions. For instance, hydrothermal aging at 800 °C for 16 h can compare with a 135,000 mile vehicle-aged SCR catalyst [19].

In this study, Cu–SAPO-34 catalysts were prepared using Cu-TEPA as Cu source and propylamine (PA) as co-template. Three key preparation parameters, including calcination temperature, Cu source and co-template amounts, were optimized systematically, and Cu–SAPO-34 catalysts with high NO*x* removal efficiency, N_2 selectivity and hydrothermal stability were synthesized successfully. By using N_2 adsorption/desorption, XRD, H_2-TPR and NH_3-TPD, the origin of the high activity and excellent hydrothermal stability was investigated in detail.

2. Experimental

2.1. Catalyst synthesis

A series of Cu–SAPO-34 catalysts was prepared using Cu-TEPA as Cu source, PA as co-template, pseudoboehmite as the Al source, 85% phosphoric acid as the P source, and fumed silica as the Si source. The molar composition of the synthesized gel was: 1Al:1 P:0.25Si:(0.03–0.20)Cu-TEPA:(1.2–1.8)PA:40H_2O. The resulting gel was transferred to an autoclave with a Teflon liner, and crystallized for 72 h at 180 °C. The crystalline products were filtered and washed with distilled water, and dried at 100 °C overnight.

In order to the investigate the effect of calcination temperature, an initial Cu–SAPO-34 sample with Cu loading of about 5% was prepared. The catalysts were then calcined in air for 5 h to remove the organic templates at temperatures of 500, 600, 700 or 800 °C, and designated as Cu_5–SAPO-34–T, where T represented the calcination temperature.

By adjusting the content of Cu-TEPA with constant PA/Al = 1.6, Cu–SAPO-34 samples with different Cu loadings can be obtained (Table 1). By changing the input of PA, with constant Cu-TEPA/Al = 0.06, Cu–SAPO-34 samples with varying properties can also be obtained (Table 2). These initial powder samples were calcined in air at 700 °C, and designated as Cu_x–SAPO-34 with *x* representing the Cu loading.

To investigate the hydrothermal stability of Cu–SAPO-34 samples, the catalysts were hydrothermally aged at 750 °C and 800 °C for 16 h in a flow of 10% H_2O/air.

2.2. NH_3-SCR activity measurement

SCR activity tests of the sieved powder catalysts were carried out in a fixed-bed quartz flow reactor at atmospheric pressure. The reaction conditions were controlled as follows: 500 ppm NO, 500 ppm NH_3, 5 vol.% O_2, balance N_2 and 500 mL/min total flow rate. During the performance tests, about 60 mg catalyst was used, yielding a rather high GHSV of 400,000 h^{-1}. The effluent gas, including NO, NH_3, NO_2, and N_2O, was continuously analyzed by an online NEXUS 670-FTIR spectrometer equipped with a heated, low volume (0.2 L) multiple-path gas cell (2 m). The FTIR spectra were collected throughout and the results were recorded when the SCR reaction reached a steady state. In this study, we defined the N_2 selectivity as the percentage of N atoms in the feed gas NO + NH_3 not changing into N_2O and NO_2 in the SCR reaction process. Then, the NO*x* conversion and N_2 selectivity were calculated according to the following equations:

$$NO_x \text{ conversion} = \left(1 - \frac{[NO]_{out} + [NO_2]_{out}}{[NO]_{in} + [NO_2]_{in}}\right) \times 100\%$$

$$N_2 \text{ selectivity} = \frac{[NO]_{in} + [NH_3]_{in} - [NO_2]_{out} - 2[N_2O]_{out}}{[NO]_{in} + [NH_3]_{in}} \times 100\%$$

2.3. Characterization

N_2 adsorption/desorption isotherms of the Cu–SAPO-34 samples were measured at −196 °C using a Quantachrome Quadrasorb SI-MP to obtain the specific surface area and pore volume. Prior to the N_2 physical adsorption, the samples were degassed at 300 °C for 5 h. Surface areas and pore volumes were determined by the t-plot method.

Powder X-ray diffraction (XRD) measurements were carried out on a computerized PANalytical X'Pert Pro diffractometer with Cu Kα (λ = 0.15406 nm) radiation. The data of 2θ from 5° to 40° were collected with the step size of 0.02°.

Temperature-programmed reduction with hydrogen (H_2-TPR) experiments were carried out on a Micromeritics AutoChem 2920 chemisorption analyzer. The interference of H_2O was eliminated by using a liquid nitrogen cold trap before the detector. 50 mg of the samples in a quartz reactor were pre-treated in air with the flow rate of 50 mL/min at 500 °C for 1 h. After the catalyst was cooled down to room temperature, H_2-TPR was performed in 10 vol.% H_2/Ar gas flow of 50 mL/min at a heating rate of 10 °C/min to 900 °C.

Table 1
Cu loadings of the Cu_x–SAPO-34 by adjusting Cu-TEPA contents in the resulting gel.

Samples	Cu-TEPA/Al	Cu, wt.%
$Cu_{2.71}$–SAPO-34	0.03	2.71
$Cu_{3.44}$–SAPO-34	0.06	3.44
$Cu_{6.62}$–SAPO-34	0.15	6.62
$Cu_{8.84}$–SAPO-34	0.20	8.84

Table 2
Properties of Cu_x–SAPO-34 samples prepared with different PA inputs in the resulting gel.

Samples	PA/Al	pH of resulting gel	Cu, wt.%	Crystalline phases
$Cu_{2.96}$–SAPO-34	1.2	6.0	2.96	Amorphous + SAPO-34
$Cu_{3.20}$–SAPO-34	1.4	7.0	3.20	Amorphous + SAPO-34
$Cu_{3.44}$–SAPO-34	1.6	8.0	3.44	SAPO-34
$Cu_{5.15}$–SAPO-34	1.8	9.5	5.15	SAPO-34

Ultraviolet visible diffuse reflectance spectrum (UV–vis–DRS) were recorded at room temperature using a Hitachi UV-3010 spectrometer equipped with a diffuse reflectance accessory in the 200–800 nm wavelength range. $BaSO_4$ was used as the reference sample.

X-ray photoelectron spectroscopy (XPS) with Al Ka radiation (1486.7 eV) was used to analyze the atomic state of copper species on the catalysts surface (Axis Ultra, Kratos Analytical Ltd). The C 1 s peak at 284.8 eV was used as an internal standard for peak position measurement.

Temperature-programmed desorption with ammonia (NH_3-TPD) experiments were performed in the same instrument as H_2-TPR, equipped with a quadrupole mass spectrometer (MKS Cirrus) to record the signals of NH_3 (m/z = 17 for NH_3). The interference of H_2O was eliminated by using a cold trap before the detector. Prior to TPD experiments, 50 mg of the samples were pre-treated in air at a flow rate of 50 mL/min at 500 °C for 1 h, and then cooled down to room temperature (30 °C). The samples were then exposed to a flow of 2500 ppm NH_3/Ar (50 mL/min) at 30 °C for 1 h, followed by Ar purging for 1 h. Finally, the temperature was raised to 900 °C in Ar at the rate of 10 °C/min.

2.4. Kinetic studies

NH_3-SCR kinetic tests over fresh and aged catalysts were evaluated in a differential reactor with 4 mm inner diameter at atmospheric pressure. About 10 mg of the catalyst diluted with 40 mg of quartz sand was loaded with a catalyst bed length of ca. 2 mm. Under the different conditions, the NO*x* conversion was kept less than 20% in the temperature range tested. To eliminate the effects of diffusion, a total gas flow rate of 500 mL/min and particle size of 40–60 mesh were used. The gas mixture was composed of 500 ppm NO, 500 ppm NH_3, 5 vol.% O_2, and the balance N_2. The effluent gas was also analyzed by an online NEXUS 670-FTIR spectrometer as described above. NO*x* reduction rates (mol/g/s) were calculated as:

$$r_{NO_x} = X_{NO_x} Y_{NO_x,in} V_{gas} / m_{cat}$$

where X_{NOx} is the NO*x* conversion, $Y_{NOx,in}$ is the NO_x molar fraction in the inlet gas, V_{gas} is the total flow rate in moles per second, and m_{cat} is the mass of the catalyst in grams.

3. Results and discussion

3.1. Effect of calcination temperature

3.1.1. NH_3-SCR activity and N_2 selectivity

The NO*x* conversion and N_2 selectivity of Cu_5–SAPO-34–T catalysts with different calcination temperatures are shown in Fig. 1. It can be observed that calcination temperature had a remarkable influence on the catalytic performance of Cu_5–SAPO-34 catalyst. Among the catalysts calcined at different temperatures, Cu_5–SAPO-34–700 exhibited superior low-temperature SCR activity and a broad temperature window for NO*x* removal, with almost 100% NO*x* conversion in the range of 250–400 °C. The steady state NO*x* conversion below 350 °C increased with increasing calcination

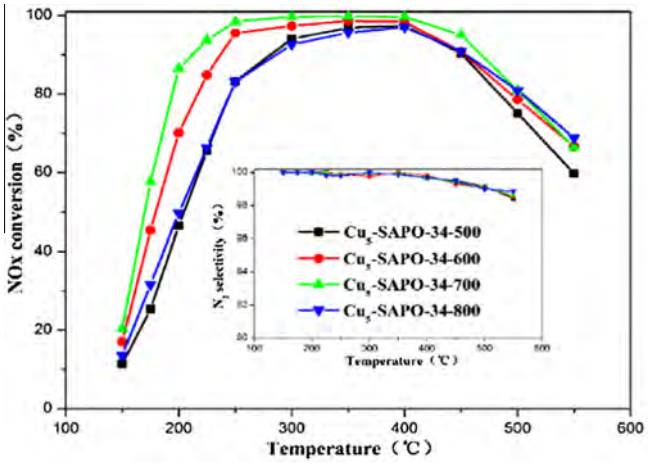

Fig. 1. NO*x* conversion and N_2 selectivity over Cu_5–SAPO-34–T samples with varied calcination temperatures.

temperature from 500 to 700 °C, and then decreased for higher calcination temperature at 800 °C. There was little effect on NH_3-SCR activity above 350 °C. The N_2 selectivity of all Cu_5–SAPO-34–T samples were higher than 98% in the whole reaction temperature range. These results suggested clearly that appropriate calcination temperature was important for the catalytic activity of Cu–SAPO-34. Gao et al. [13] studied solid-state reaction between SAPO-34 and CuO under different calcination temperatures and times and found that a portion of CuO (~67%) converted to isolated Cu^{2+} ions after the SSIE treatment at 800 °C for 16 h. It suggested that the copper species in Cu–SAPO-34 can be redistributed to yield an active catalyst upon high temperature treatment. However, copper species distribution of Cu_5–SAPO-34–T samples did not change distinctly (Fig. S1), suggesting that the deNO*x* catalytic activity differences among Cu_5–SAPO-34–T samples mainly attributed to the varying structural properties.

Furthermore, the NO*x* conversion over hydrothermally aged Cu_5–SAPO-34–T catalysts was investigated. As shown in Fig. 2(c), the deNO*x* catalytic activity of aged Cu_5–SAPO-34–700 (750 °C–16 h) did not significantly change at low temperatures and slightly decreased at high temperatures. By comparing with all the fresh and aged samples, it was seen clearly that the Cu_5–SAPO-34–700 showed excellent SCR activity and hydrothermal stability, while the Cu_5–SAPO-34–800 performed inferiorly especially under harsh treatment.

3.1.2. N_2 adsorption/desorption

Table 3 shows the specific surface area and pore volume of the Cu_5–SAPO-34–T samples calcined at different temperatures. The specific surface area of the Cu–SAPO-34 catalysts were strongly affected by the calcination temperatures and increased monotonically from 501.1 m^2/g to 566.6 m^2/g with the calcination temperature rising from 500 to 700 °C. When catalysts were calcined at higher temperatures (800 °C), the surface area decreased. It is widely accepted that the surface area of zeolites decreases with the increase of the calcination temperatures, as observed for Fe-

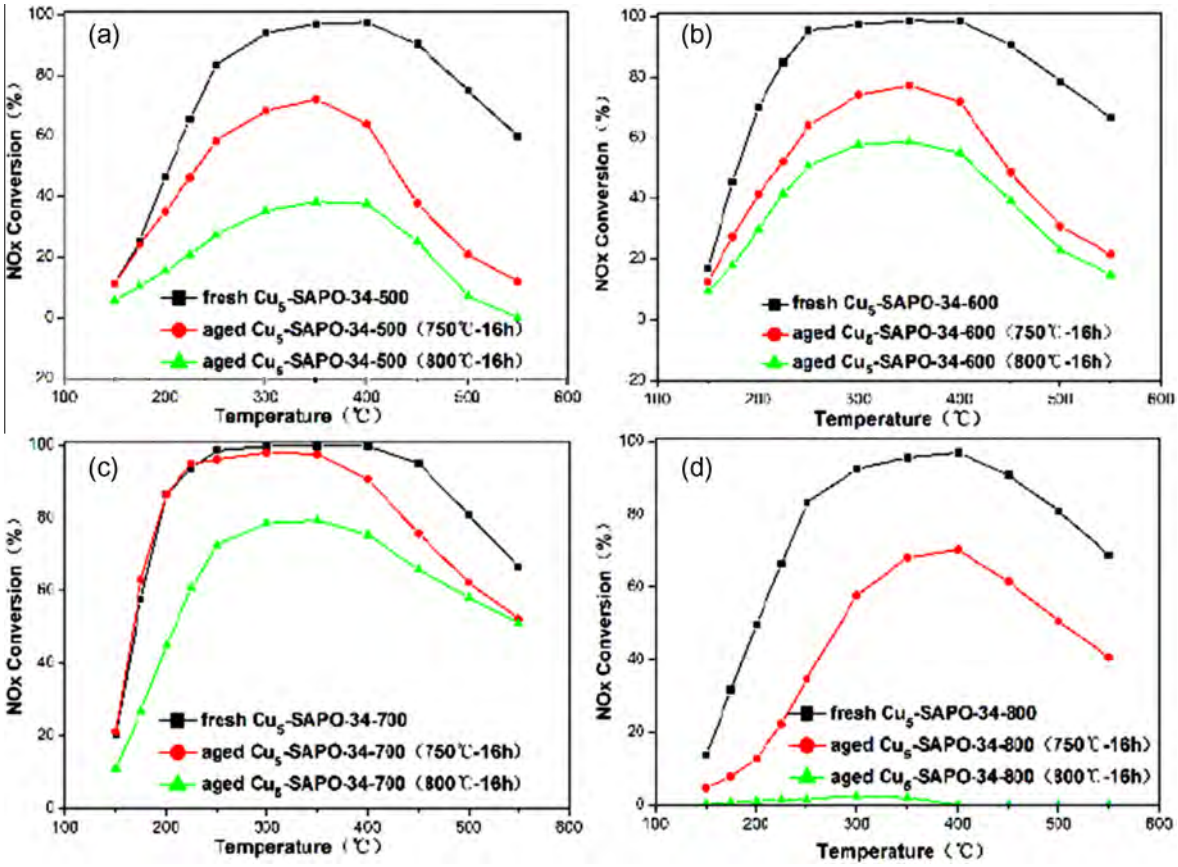

Fig. 2. NO*x* conversion over fresh and aged Cu_5–SAPO-34–T samples with varied calcination temperatures.

Table 3
Properties of the Cu_5–SAPO-34–T samples calcined at different temperatures.

Samples	Specific surface area, m^2/g	Pore volume, cm^3/g
Cu_5–SAPO-34–500	501.1	0.26
Cu_5–SAPO-34–600	506.8	0.26
Cu_5–SAPO-34–700	566.6	0.29
Cu_5–SAPO-34–800	480.7	0.25

HBEA and Mo/HZSM-5 [20,21]. However, the Cu–SAPO-34 catalyst in the present study differed from those zeolites possibly due to the pore structure forming gradually during the calcination process and reached a maximum. Because of the same Cu loading and similar copper species distribution, the activity of Cu_5–SAPO-34–T eliminated the effect of Cu species which could influence the SCR activity. As shown in Fig. 1, the Cu_5–SAPO-34–700 sample with the largest surface area and pore volume, which can supply the largest inner surface area for the SCR reaction, showed the highest NO*x* conversion in the SCR reaction. Li et al. [22] also indicated that the excellent catalytic activity was attributed to the large specific surface area.

3.1.3. Powder XRD

To further confirm the peak intensity changes and the integrity of the CHA zeolite structure under different calcination temperatures, the XRD patterns of Cu_5–SAPO-34–T samples were obtained and are shown in Fig. 3. Typical CHA structure diffraction peaks (see http://www.iza-structure.org/databases for standard XRD patterns) were observed in all samples. Gao et al. [13] reported that a weak diffraction feature of SiO_2 appeared for the sample aged at 800 °C for 1, 5 and 16 h, suggesting some decomposition. Nevertheless, there was no evident that CHA structure decomposed for sample calcined at 800 °C for 5 h in our work, indicating that the physical structure of Cu_5–SAPO-34–T sample was stable under the current calcination temperatures.

Increase in intensity of the XRD peaks represented the increase in the crystallinity [23]. The crystallinity increased with increasing calcination temperature from 500 to 700 °C, and then declined when the calcination temperature was 800 °C, which conformed well with the trend of SCR activity. Ye et al. [24] reported that the Ag–SAPO-34 which had high degree of crystallinity, showed good catalytic activity. The Cu_5–SAPO-34 catalyst with the highest degree of crystallization, surface area and pore volume could be obtained by calcination at an optimum temperature of 700 °C. Hence, the calcination temperature was chosen as 700 °C for further investigations in the present study.

3.2. Effects of Cu source and co-template

3.2.1. NH_3-SCR activity and N_2 selectivity

SCR performance tests were conducted on samples with different Cu source contents in the resulting gel are shown in Fig. 4(a). The $Cu_{2.71}$–SAPO-34 sample containing the lowest Cu loading showed moderate activity, indicating that more active copper species were needed. When the Cu loading was 3.44%, the NO*x* conversion increased to 90% at 200 °C and maintained that level until 400 °C with the N_2 selectivity of more than 98% in the whole temperature range. With further increase of the Cu loading, the activity levelled off below 350 °C. However, at high temperatures (350–550 °C), the NO*x* conversion decreased rapidly when the Cu loading was above 3.44%, and a dramatic decline of NO*x* conversion and N_2 selectivity was observed over the $Cu_{8.84}$–SAPO-34 sample.

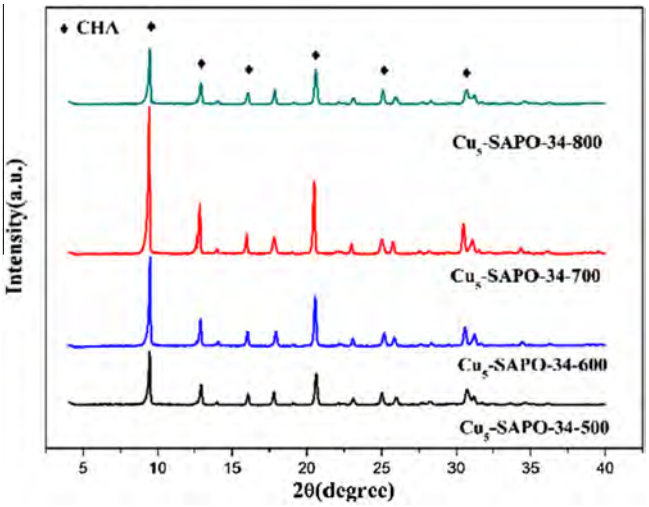

Fig. 3. Powder XRD patterns of Cu_5–SAPO-34–T samples with varied calcination temperatures.

Most researchers consider that the active sites for NH_3-SCR reactions are likely to be isolated Cu^{2+} ions at exchange sites [11,16,25,26] and that the CuO species could lead to non-selective oxidation of NH_3 and decreased NH_3-SCR activity at high temperatures [14,27,28]. Table 4 shows that the amount of Cu^{2+} ions increased from 1.35% to 4.69% along with the improvement of the SCR activity below 350 °C. One the other hand, the amount of CuO increased from 0.35% to 2.07% along with the decrease of the SCR activity above 350 °C. With Cu loading from 3.44% to 6.62%, the NO*x* conversion did not obviously improve, indicating that active sites were almost saturated on the $Cu_{3.44}$–SAPO-34 sample. The result showed that, there existed the best Cu loading rather than the Cu loading was the higher the better.

Properties of Cu_x–SAPO-34 samples prepared with different PA inputs in the resulting gel are shown in Table 2. With the increase of PA/Al ratio from 1.2 to 1.8, the pH of the gel increased from 6.0 to 9.5 with Cu loading increasing from 2.96% to 5.15%. The template agent such as PA used to fill the CHA framework and direct the synthesis of Cu–SAPO-34, is a kind of strong alkalogenic organic amine. Therefore, the input of PA greatly influenced the chemical environment such as pH value of the resulting gel which could affect the degree of solubility and polymerization of raw materials and further impact the crystalline phase of the zeolite. White et al. [29] indicated that zeolite synthesis is the process of inorganic oxide polymerization and deprotonation which depend greatly on the pH value using density functional theory (DFT). Lower pH value led to decreased solubility of amorphous silica in the silicate dimerisation reactions. As a result of shortage of the nuclear material in the solution at low pH, amorphous phase was obtained. Hence, Cu–SAPO-34 catalysts were only achieved at appropriate pH value.

As is shown in Fig. 4(b), with the increasing of PA inputs, the deNO*x* catalytic activity of Cu_x–SAPO-34 samples improved below 350 °C and showed decline trend as a whole at high temperatures. Although the $Cu_{5.15}$–SAPO-34 (pH = 9.5) sample performed better than the $Cu_{3.44}$–SAPO-34 (pH = 8.0) sample below 350 °C, it cannot be concluded that both Cu–SAPO-34 samples were promising candidates for NH_3-SCR, since an excellent catalyst should possess high hydrothermal stability. Hence, hydrothermal treatments were conducted on the two samples to choose the better candidate, and further, the optimum synthesis condition, as shown in Section 3.3.

3.2.2. Powder XRD

The crystal structures of Cu_x–SAPO-34 samples were verified *via* XRD measurements. As shown in Fig. 5, Cu_x–SAPO-34 maintained the CHA framework structure basically after high temperature calcination. However, two extra peaks at 35.29° and 38.49° related to CuO phases were observed in $Cu_{6.62}$–SAPO-34 and $Cu_{8.84}$–SAPO-34 [30,31]. In the Cu_x–SAPO-34 with low Cu loading (<5.15 wt.%), no Cu-related phases were observed in the XRD patterns, suggesting that copper oxide was present in a highly dispersed amorphous state. The result further proved that too much CuO was present in the Cu_x–SAPO-34 catalysts with high Cu loadings. $Cu_{2.96}$–SAPO-34 sample exhibited the lowest crystalline nature mainly due to the mixture of SAPO-34 and amorphous material which was prepared at inappropriate pH value of 6.0.

3.3. The origin of the high hydrothermal stability of Cu–SAPO-34

3.3.1. NH_3-SCR activity

The NO*x* conversion over fresh and hydrothermally aged $Cu_{3.44}$–SAPO-34 is shown in Fig. 6(a). After 750 °C hydrothermal aging for 16 h, the SCR activity over the whole temperature range slightly increased, reaching ca. 90% at 200 °C, and maintained this level until 450 °C. Even after hydrothermal aging at 800 °C for 16 h, $Cu_{3.44}$–SAPO-34 still maintained excellent SCR activity, exceeding 90% from 225 to 400 °C. The SCR performance of fresh and hydrothermally aged $Cu_{5.15}$–SAPO-34 is shown in Fig. 6(b). The

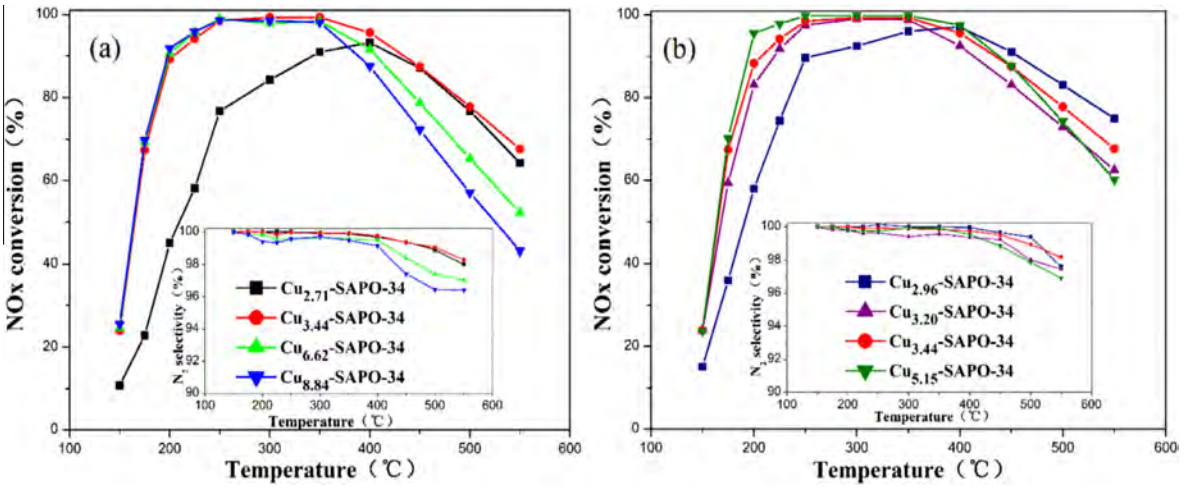

Fig. 4. NO*x* conversion and N_2 selectivity over Cu_x–SAPO-34 samples.

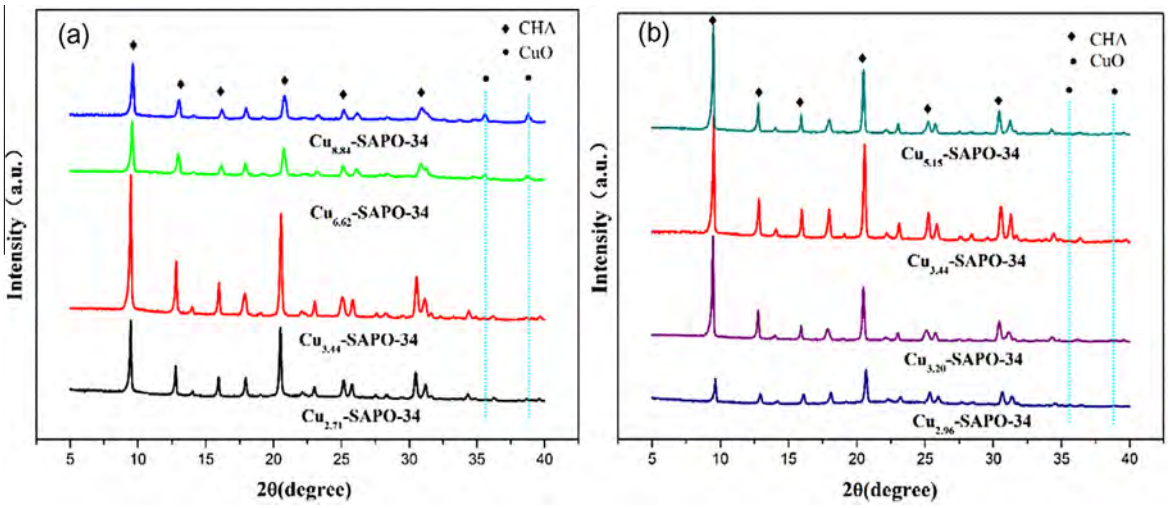

Fig. 5. XRD patterns of Cu_x–SAPO-34 samples.

results showed that the NO*x* conversion above 350 °C decreased slightly over $Cu_{5.15}$–SAPO-34 after hydrothermal aging at 750 °C for 16 h, whereas hydrothermal aging at 800 °C for 16 h deactivated $Cu_{5.15}$–SAPO-34 completely. It was recognized that compared to the high Cu loading sample, the relatively low Cu loading sample was more resistant to relatively harsh hydrothermal treatment. It was speculated that high copper loading might cause the accumulation of copper species, forming CuO clusters, leading to structural instability.

3.3.2. H_2-TPR

The H_2-TPR characterization was carried out to probe the distribution and reducibility of copper species. Fig. 7 shows that multiple Cu species coexist in the fresh and aged $Cu_{3.44}$–SAPO-34 and $Cu_{5.15}$–SAPO-34 samples. According to the literature [30,32–34], the low temperature and high temperature peaks were assigned to the $Cu^{2+} \rightarrow Cu^{+}$ and $Cu^{+} \rightarrow Cu^{0}$ reduction steps, respectively. The reduction of CuO took place in a one-step mechanism ($CuO \rightarrow Cu^{0}$) and occurred in the same temperature range as the reduction of Cu^{2+} to Cu^{+} (low temperature peak). Therefore, 210–250 °C was assigned to the reduction of isolated Cu^{2+} to Cu^{+}, and 360–470 °C was attributed to the reduction of CuO to Cu^{0}. The third peak at 670–770 °C was attributed to the reduction of Cu^{+} to Cu^{0}. EPR was an excellent technique for identifying the coordination environment of isolated Cu^{2+} ions, because all the other Cu species (CuO or Cu^{+}) were EPR silent [35,36]. By analyzing the hyperfine features of the hydrated $Cu_{3.44}$–SAPO-34 sample, g// = 2.380 and A = 130.5 G was obtained (Fig. S3). Zamadics et al. [35] reported that EPR signal (g// = 2.381, A = 143 G) in hydrated Cu–SAPO-34 could be assigned to Cu^{2+} located in the six-membered-ring as a complex $Cu(O_F)_3(H_2O)_3$. The similar EPR signals for Cu-CHA catalysts reported by others [26,37] were also suggested to be this type of species, such as g// = 2.39 with A = 111 G and g// = 2.394 with A = 131 G. Thus, this EPR signal should be due to the isolated Cu^{2+} located in the six-membered-ring for hydrated $Cu_{3.44}$–SAPO-34 catalyst. Through integrating the H_2 consumption peak areas, it was concluded that the first and the third reduction peaks were not equal for all samples, suggesting that the isolated Cu^{2+} ions might follow a one-step reduction mechanism ($Cu^{2+} \rightarrow Cu^{+}$). Some Cu^{2+} ions are too stable to be reduced to Cu^{0} at temperatures below 900 °C. H_2 consumption peaks at 670–770 °C have been attributed to the reduction of Cu^{+} to Cu^{0}, either due to the Cu^{+} formed from the first step of reduction of isolated Cu^{2+} or due to the Cu^{+} originally existing in the framework of Cu–SAPO-34 [14,26].

What's more, the copper species distribution changed after hydrothermal aging over $Cu_{3.44}$–SAPO-34 and $Cu_{5.15}$–SAPO-34. It was reported that hydrothermal treatment of the Cu–SAPO-34 catalyst led to the migration of copper species [28,31,38], and the changes in copper oxidation states and its coordination environment directly affect the SCR activity. The H_2-TPR results showed that ~6% CuO in $Cu_{3.44}$–SAPO-34 transformed to isolated Cu^{2+} after hydrothermal aging at 750 °C for 16 h (Table S1). As a result, the SCR activity increased over the aged $Cu_{3.44}$–SAPO-34 sample due to the presence of a larger amount of active Cu^{2+} ions. On the other hand, the copper species transformed from copper ions (Cu^{2+} and Cu^{+}) to CuO on the aged $Cu_{3.44}$–SAPO-34 (800 °C–16 h) and aged $Cu_{5.15}$–SAPO-34 (750 °C–16 h), leading to the decline of the SCR activity.

3.3.3. UV–vis–DRS

As shown in Fig. 8, UV–vis–DRS spectra were obtained to verify the nature of copper species of fresh and aged $Cu_{3.44}$–SAPO-34 samples. For fresh and aged $Cu_{3.44}$–SAPO-34 samples, the charge transfer band at around 230 nm can be assigned to the transfer from $O_{SAPO-34}$ to isolated Cu^{+}/Cu^{2+} ions [39,40]. A broad band in

Table 4
The Cu species distribution on the Cu_x–SAPO-34 samples with different Cu loadings.

Catalysts	NO*x* conversion at 200 °C, %	[a]Cu^{2+}, wt.%	NO*x* conversion at 450 °C, %	[a]CuO, wt.%
$Cu_{2.71}$–SAPO-34	45	1.35	87	0.35
$Cu_{3.44}$–SAPO-34	90	1.93	87	0.58
$Cu_{6.62}$–SAPO-34	91	3.55	78	1.45
$Cu_{8.84}$–SAPO-34	92	4.69	72	2.07

[a] Calculated by the amount of H_2 consumption from H_2-TPR results (Fig. S2).

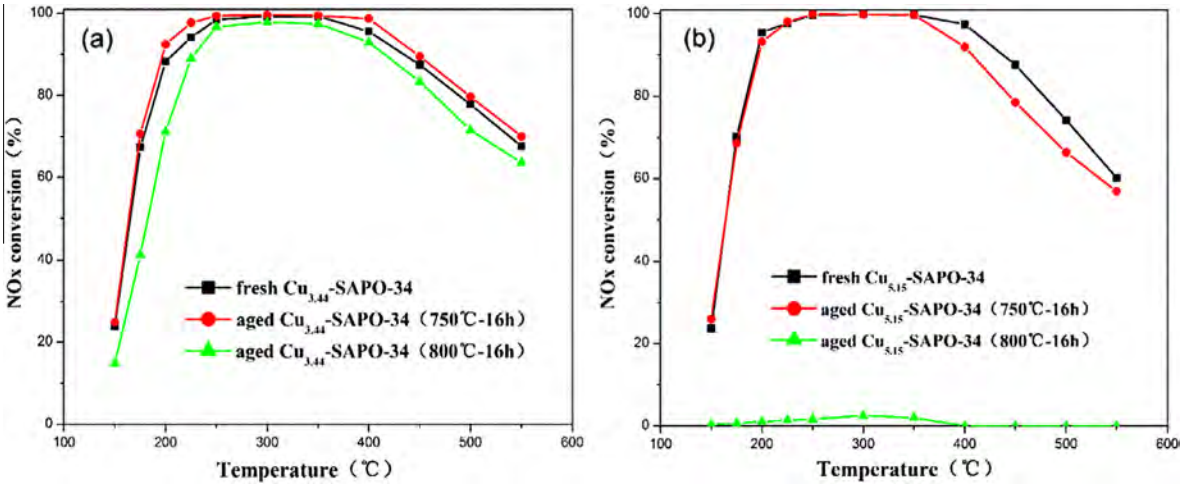

Fig. 6. NO*x* conversion over the fresh and aged samples (a) $Cu_{3.44}$–SAPO-34 (b) $Cu_{5.15}$–SAPO-34.

the region of 600–800 nm was attributed to the electron d–d transitions of Cu^{2+} in distorted octahedral coordination surrounded by oxygen in CuO particles [31,41]. Compared with the results for the fresh sample, an increase in intensity of the band at 230 nm and a decrease in intensity of the band at 600–800 nm can be observed for 750 °C-aged $Cu_{3.44}$–SAPO-34. This indicated that the copper oxide species on the external surface of $Cu_{3.44}$–SAPO-34 could transform to copper ions and migrate into the cages of SAPO-34 during the hydrothermal process at 750 °C for 16 h, rather than aggregating to form larger clusters. In the case of the sample aged at 800 °C, the changes in the spectrum suggested the increase of CuO particles and decrease of isolated Cu^{2+} ions. The UV–vis–DRS results were in accordance with the H_2-TPR results.

3.3.4. XPS

The XPS results of the fresh and aged $Cu_{3.44}$–SAPO-34 samples are shown in Fig. 9. Cu $2p_{3/2}$ and Cu $2p_{1/2}$ peaks were observed in the ranges of 932.0–938.0 and 952.0–958.0 eV, respectively. The Cu $2p_{3/2}$ peak around 935.8 eV as well as the satellite peak around 940.0–948.0 eV is used as a characteristic to determine Cu^{2+} [42,43]. The peaks of Cu $2p_{3/2}$ are further discussed in terms of the effect of hydrothermal treatments on the Cu valence state on the surface of the catalysts. It can be seen that the satellite peak around 940.0–948.0 eV was more obvious, indicating more isolated Cu^{2+} on the surface of $Cu_{3.44}$–SAPO-34 after hydrothermal aging at 750 °C which led to the performance improvement for NO*x* removal to a certain degree. However, the peak at around 935.8 eV of aged $Cu_{3.44}$–SAPO-34 after aging at 800 °C decreased, indicating low Cu^{2+} concentration, which may be associated with the agglomeration of CuO [42,44] and in accordance with the H_2-TPR and UV–vis–DRS results, revealing the mechanism of deactivation during high temperature hydrothermal treatment.

3.3.5. Powder XRD

Fig. 10 shows the XRD patterns of the fresh and aged $Cu_{3.44}$–SAPO-34 and $Cu_{5.15}$–SAPO-34 samples. Except for the $Cu_{5.15}$–

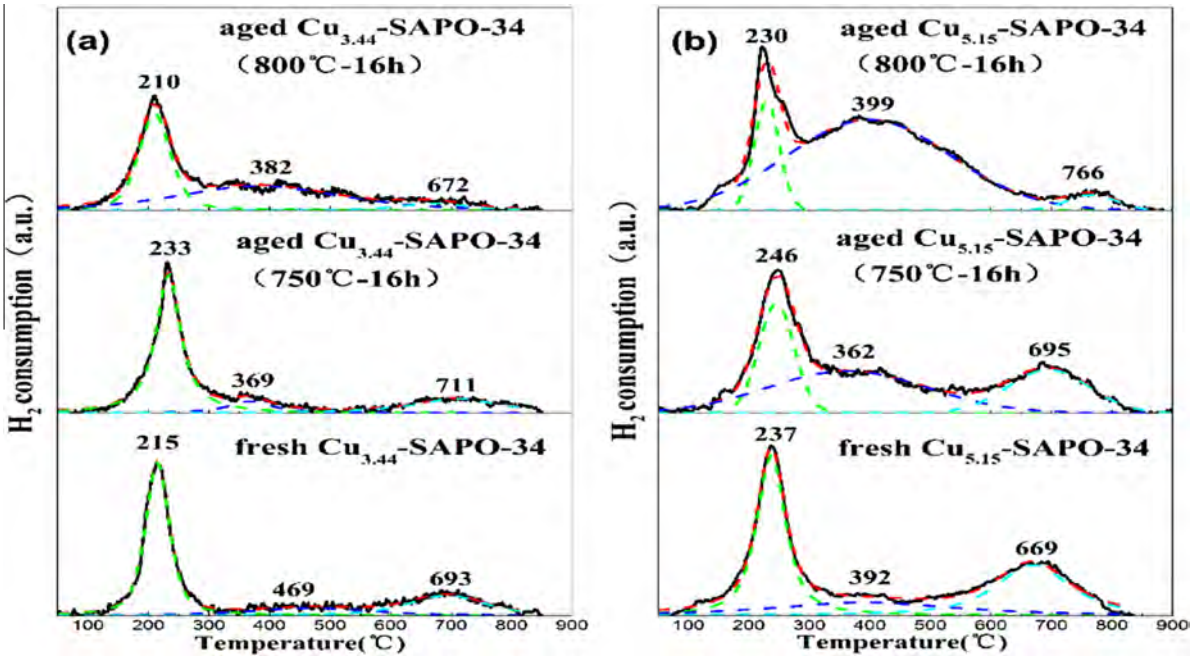

Fig. 7. H_2-TPR patterns of fresh and aged samples (a) $Cu_{3.44}$–SAPO-34 (b) $Cu_{5.15}$–SAPO-34.

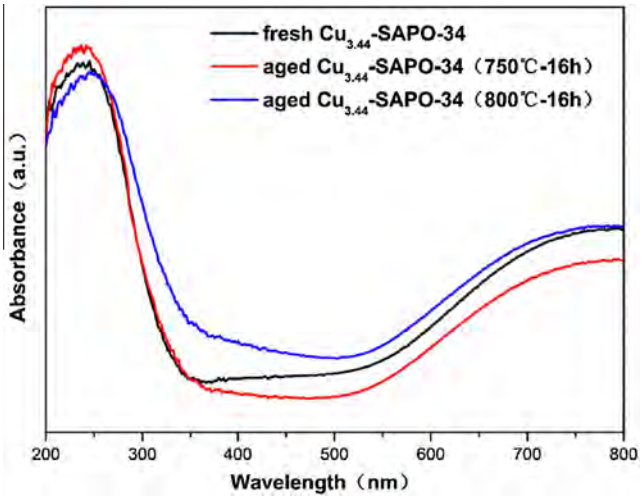

Fig. 8. UV–vis–DRS spectra of fresh and aged $Cu_{3.44}$–SAPO-34 samples.

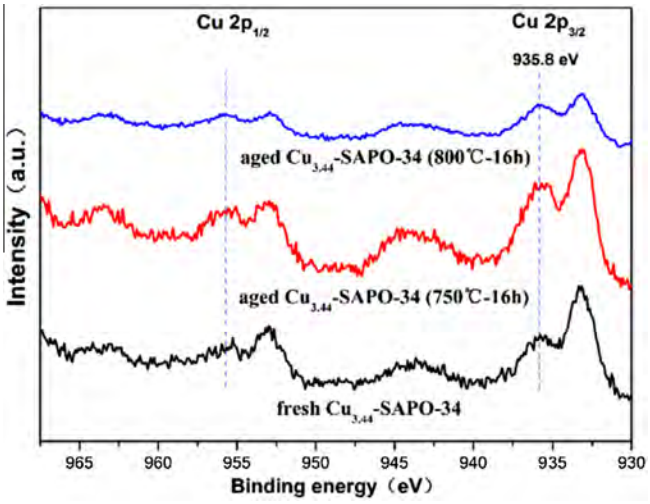

Fig. 9. XPS results of fresh and aged $Cu_{3.44}$–SAPO-34 samples.

SAPO-34 sample aged at 800 °C for 16 h, all the other catalysts maintained the CHA zeolite structure. The collapse of the CHA framework resulted in the completely deactivation of the $Cu_{5.15}$–SAPO-34 catalyst. On the contrary, hydrothermal treatment at 750 °C for 16 h had a negligible effect on the CHA structure of $Cu_{3.44}$–SAPO-34, and the treatment under the higher temperature of 800 °C could not destroy the CHA structure. This was consistent with the moderate decrease in specific surface area and pore volume on aged $Cu_{3.44}$–SAPO-34 samples measured by N_2 adsorption/desorption as shown in Table S2. On the other hand, the $Cu_{5.15}$–SAPO-34 catalyst appeared to be more vulnerable by hydrothermal treatment. After the CHA structure collapsed, little pore structure was left on 800 °C-aged $Cu_{5.15}$–SAPO-34. The Hydrothermal treatments indeed caused some damage to the physical structure probably due to the accumulation of copper species which had an adverse effect on the stability of the structure and led to lower NH_3-SCR activity, but this effect was not very significant on the $Cu_{3.44}$–SAPO-34 catalyst, indicating that this catalyst is a prospective candidate for industrial applications in the near future.

3.3.6. Acidity

To determine the density and strength of acid sites in the fresh and aged $Cu_{3.44}$–SAPO-34 and $Cu_{5.15}$–SAPO-34 catalysts, NH_3-TPD measurements were carried out (Fig. 11). For the fresh $Cu_{3.44}$–SAPO-34 sample, three NH_3 desorption peaks were observed. The peak (A) at 114 °C was found to be related to surface hydroxyl groups (Si–OH and P–OH). The peak (B) at 161 °C could be assigned to the weak structural Brønsted acid sites, whereas the peak (C) could be assigned to the strong structural Brønsted acid sites and Lewis acid sites (Si–OH–Al and Cu^{2+}) [14,45,46]. The distinction between acid sites present on the zeolite surface and those generated by deposition of copper can be realized by comparison of NH_3-TPD results for Cu–SAPO-34 with different Cu loadings. As shown in Fig. S4, with the increase of Cu loading the absolute intensities of the peak between 230 and 320 °C increased and the absolute intensities of the peak between 320 and 500 °C decreased. Wang et al. [14] reported that Lewis acid sites can be created via Cu occupation of Brønsted acid sites in the pores. Wang et al. [47] also showed that the Cu^{2+} species can substitute for the proton (Si–OH–Al) of SAPO-34 supports. Hence, we deduced that the peak between 230 and 320 °C can represent the Lewis acid sites generated by deposition of copper, which increased with increasing Cu

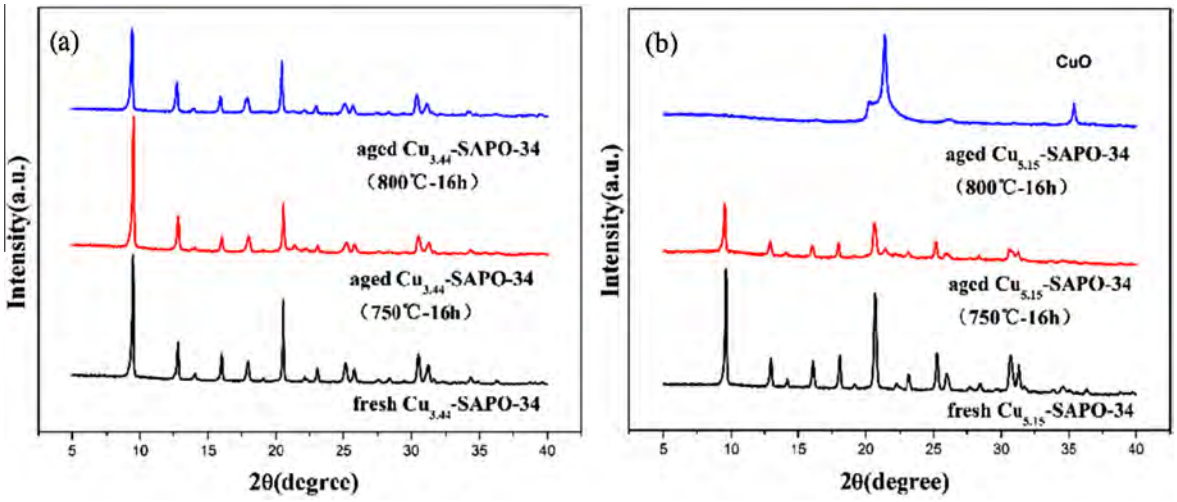

Fig. 10. XRD patterns of the fresh and aged samples (a) $Cu_{3.44}$–SAPO-34 (b) $Cu_{5.15}$–SAPO-34.

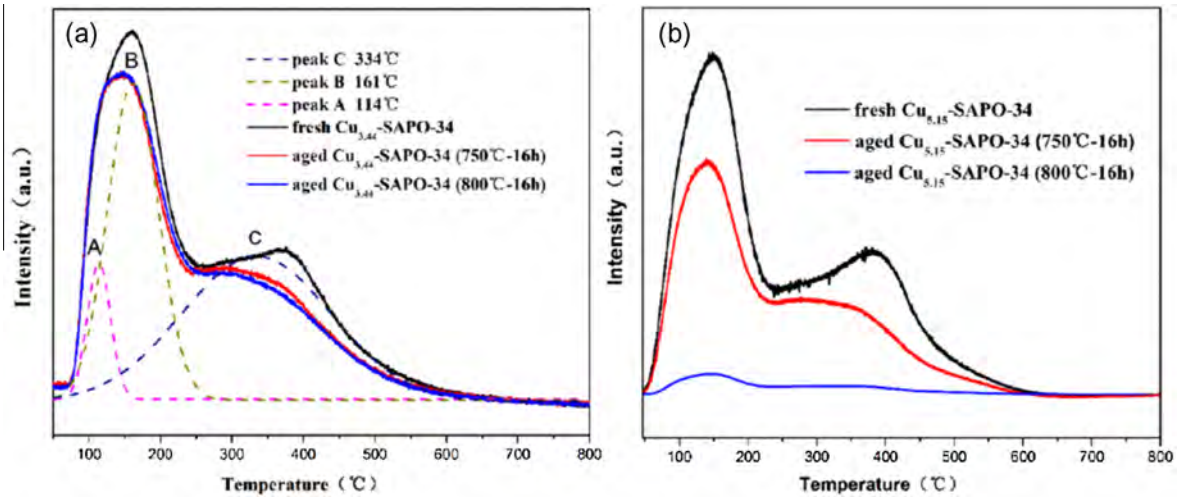

Fig. 11. NH_3-TPD over fresh and aged $Cu_{3.44}$–SAPO-34 and $Cu_{5.15}$–SAPO-34 samples.

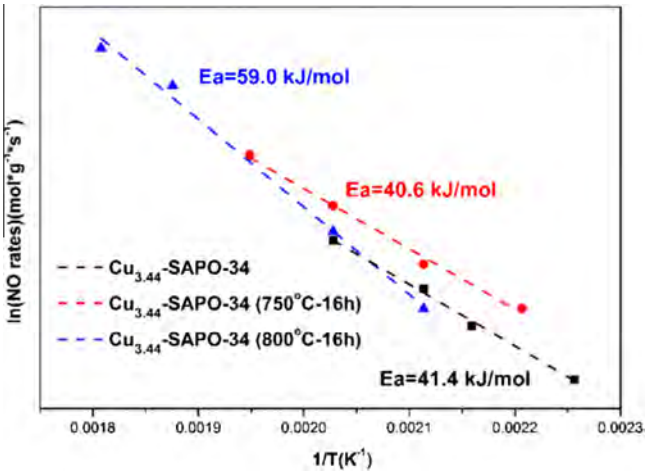

Fig. 12. Kinetic results of NH_3-SCR over the fresh and aged $Cu_{3.44}$–SAPO-34 samples.

loadings. The decline of the peak between 320 and 500 °C showed a reduction in the number of strong structural Brønsted acid sites. After harsh aging treatment, a slight decrease in the density of the acid sites was observed, indicating that the $Cu_{3.44}$–SAPO-34 sample maintained most of the surface and structural hydroxyl groups. The Lewis acid sites generated by Cu^{2+} was little affected by hydrothermal treatment. However, aging treatment decreased the density of acid sites in $Cu_{5.15}$–SAPO-34 more significantly than that in $Cu_{3.44}$–SAPO-34. The acidity in $Cu_{5.15}$–SAPO-34 after aging at 800 °C for 16 h were destroyed completely after such severe treatment.

3.3.7. Kinetic studies

In order to further prove the conclusions gained from the NH_3-SCR tests, H_2-TPR and NH_3-TPD results, some kinetics studies were carried out over fresh and aged $Cu_{3.44}$–SAPO-34 catalysts. The apparent activation energy (Ea) was estimated using the data obtained in the temperature range (170–280 °C) where NO*x* conversions showed notable differences based on the Arrhenius plot of the rate (R) versus inverse temperature for NO (Fig. 12). The results revealed that hydrothermal treatment at 750 °C declined the Ea over $Cu_{3.44}$–SAPO-34 from 41.4 to 40.6 kJ/mol. Otherwise, hydrothermal treatment at 800 °C increased the Ea over $Cu_{3.44}$–SAPO-34 from 41.4 to 59.0 kJ/mol. Therefore, the higher performance of NH_3-SCR over the aged $Cu_{3.44}$–SAPO-34 (750 °C–16 h) catalyst correlated well with its lower activation barrier. The hydrothermal treatment of 800 °C over $Cu_{3.44}$–SAPO-34 increased the apparent activation energy, thereby decreasing the activity of NO*x* reduction.

4. Conclusion

By using N_2 adsorption/desorption, XRD, H_2-TPR, UV–vis–DRS, XPS and NH_3-TPD, it can be concluded that the NH_3-SCR activity and hydrothermal resistivity mainly depend on the framework pore properties, stability of the structure, copper species distribution and acidity of Cu–SAPO-34. With the increasing calcination temperature, the surface area, pore volume and structure crystallinity increased from 500 to 700 °C and then declined at 800 °C. When calcined at 700 °C, the Cu–SAPO-34 catalyst with copper loading ca. 3.44% performed optimal NH_3-SCR activity. Additionally, >90% NO*x* conversion can be maintained from 225 to 400 °C over $Cu_{3.44}$–SAPO-34 catalyst after hydrothermal aging treatment at 800 °C for 16 h, indicating that $Cu_{3.44}$–SAPO-34 catalyst is a promising candidate for industrial application.

Three types of copper species were observed on Cu–SAPO-34 sample, including isolated Cu^{2+}, CuO and Cu^{+} ions. Hydrothermal aging at 750 °C led to the migration of CuO to isolated Cu^{2+} and an increase in the number of the active sites, which resulted in better NH_3-SCR performance over the aged $Cu_{3.44}$–SAPO-34 catalyst than the fresh catalyst. Meanwhile, the results of kinetics studies indicated that the apparent activation energy of aged $Cu_{3.44}$–SAPO-34 (750 °C–16 h) was lower than the fresh sample. Therefore, the maintenance of isolated Cu^{2+}, the crystallinity and acidity as well as the low activation barrier were the origin of a high hydrothermal stability for the Cu–SAPO-34 catalyst.

Acknowledgements

This work was financially supported by the National Natural Science Foundation of China (51278486, 51578536, 21303247).

Appendix A. Supplementary data

Supplementary data associated with this article can be found, in the online version, at http://dx.doi.org/10.1016/j.cej.2016.02.086.

References

[1] T.V. Johnson, Review of diesel emissions and control, Int. J. Engine Res. 10 (2009) 275–285.
[2] J.A. Sullivan, J. Cunningham, M.A. Morris, K. Keneavey, Conditions in which Cu-ZSM-5 outperforms supported vanadia catalysts in SCR of NOx by NH_3, Appl. Catal. B 7 (1995) 137–151.
[3] H. Choi, S.-W. Ham, I.-S. Nam, Y.G. Kim, Honeycomb reactor washcoated with mordenite type zeolite catalysts for the reduction of NOx by NH_3, Ind. Eng. Chem. Res. 35 (1996) 106–112.
[4] M.L.M.D. Oliveira, C.M. Silva, M.-T. Ramon, T.L. Farias, J.-L. Antonio, R.-C. Enrique, A study of copper-exchanged mordenite natural and ZSM-5 zeolites as SCR–NOx catalysts for diesel road vehicles: simulation by neural networks approach, Appl. Catal. B 88 (2009) 420–429.
[5] M. Colombo, I. Nova, E. Tronconi, A comparative study of the NH_3-SCR reactions over a Cu-zeolite and a Fe-zeolite catalyst, Catal. Today 151 (2010) 223–230.
[6] J.H. Baik, S.D. Yim, I.-S. Nam, Y.S. Mok, J.-H. Lee, B.K. Cho, S.H. Oh, Control of NOx emissions from diesel engine by selective catalytic reduction (SCR) with urea, Top. Catal. 30–31 (2004) 37–41.
[7] H. Sjövall, L. Olsson, E. Fridell, R.J. Blint, Selective catalytic reduction of NOx with NH_3 over Cu-ZSM-5—the effect of changing the gas composition, Appl. Catal. B 64 (2006) 180–188.
[8] J. Park, H. Park, J. Baik, I. Nam, C. Shin, J. Lee, B. Cho, S. Oh, Hydrothermal stability of CuZSM5 catalyst in reducing NO by NH_3 for the urea selective catalytic reduction process, J. Catal. 240 (2006) 47–57.
[9] D.W. Fickel, E. D'Addio, J.A. Lauterbach, R.F. Lobo, The ammonia selective catalytic reduction activity of copper-exchanged small-pore zeolites, Appl. Catal. B 102 (2011) 441–448.
[10] J.H. Kwak, D. Tran, S.D. Burton, J. Szanyi, J.H. Lee, C.H.F. Peden, Effects of hydrothermal aging on NH_3-SCR reaction over Cu/zeolites, J. Catal. 287 (2012) 203–209.
[11] U. Deka, L.-G. Ines, S.J. Warrender, A.L. Picone, P.A. Wright, B.M. Weckhuysen, A.M. Beale, Changing active sites in Cu-CHA catalysts: deNO(x) selectivity as a function of the preparation method, Microporous Mesoporous Mater. 166 (2013) 144–152.
[12] F. Gao, E.D. Walter, N.M. Washton, J. Szanyi, C.H.F. Peden, Synthesis and evaluation of Cu-SAPO-34 catalysts for ammonia selective catalytic reduction. 1. Aqueous solution ion exchange, ACS Catal. 3 (2013) 2083–2093.
[13] F. Gao, E.D. Walter, N.M. Washton, J. Szanyi, C.H.F. Peden, Synthesis and evaluation of Cu/SAPO-34 catalysts for NH_3-SCR 2: solid-state ion exchange and one-pot synthesis, Appl. Catal. B 162 (2015) 501–514.
[14] D. Wang, L. Zhang, J. Li, K. Kamasamudram, W.S. Epling, NH_3-SCR over Cu/SAPO-34 – zeolite acidity and Cu structure changes as a function of Cu loading, Catal. Today 231 (2014) 64–74.
[15] L. Ren, L. Zhu, C. Yang, Y. Chen, Q. Sun, H. Zhang, C. Li, F. Nawaz, X. Meng, F.S. Xiao, Designed copper-amine complex as an efficient template for one-pot synthesis of Cu-SSZ-13 zeolite with excellent activity for selective catalytic reduction of NOx by NH_3, Chem. Commun. (Camb) 47 (2011) 9789–9791.
[16] L. Xie, F. Liu, L. Ren, X. Shi, F.S. Xiao, H. He, Excellent performance of one-pot synthesized Cu-SSZ-13 catalyst for the selective catalytic reduction of NOx with NH_3, Environ. Sci. Technol. 48 (2014) 566–572.
[17] M.-F. Raquel, M. Moliner, C. Franch, A. Kustov, A. Corma, Rational direct synthesis methodology of very active and hydrothermally stable Cu-SAPO-34 molecular sieves for the SCR of NOx, Appl. Catal. B 127 (2012) 273–280.
[18] M.-F. Raquel, M. Moliner, P. Concepcion, J.R. Thogersen, A. Corma, Synthesis, characterization and reactivity of high hydrothermally stable Cu-SAPO-34 materials prepared by "one-pot" processes, J. Catal. 314 (2014) 73–82.
[19] S.J. Schmieg, S.H. Oh, C.H. Kim, D.B. Brown, J.H. Lee, C.H.F. Peden, D.H. Kim, Thermal durability of Cu-CHA NH_3-SCR catalysts for diesel NOx reduction, Catal. Today 184 (2012) 252–261.
[20] L. Ma, J. Li, H. Arandiyan, W. Shi, C. Liu, L. Fu, Influence of calcination temperature on Fe/HBEA catalyst for the selective catalytic reduction of NOx with NH_3, Catal. Today 184 (2012) 145–152.
[21] P.L. Tan, Y.L. Leung, S.Y. Lai, C.T. Au, The effect of calcination temperature on the catalytic performance of 2 wt.% Mo/HZSM-5 in methane aromatization, Appl. Catal. A 228 (2002) 115–125.
[22] J. Li, Z. Song, P. Ning, Q. Zhang, X. Liu, H. Li, Z. Huang, Influence of calcination temperature on selective catalytic reduction of NOx with NH_3 over CeO_2-ZrO_2-WO_3 catalyst, J. Rare Earth 33 (2015) 726–735.
[23] W.P.S.L. Wijesinghe, M.M.M.G.P.G. Mantilaka, E.V.A. Premalal, H.M.T.U. Herath, S. Mahalingam, M. Edirisinghe, R.P.V.J. Rajapakse, R.M.G. Rajapakse, Facile synthesis of both needle-like and spherical hydroxyapatite nanoparticles: effect of synthetic temperature and calcination on morphology, crystallite size and crystallinity, Mater. Sci. Eng. C 42 (2014) 83–90.
[24] W. Le-fu, Fu Ye, Tan Yu-xin, Effects of crystallization conditions on the crystallinity and catalytic activity of SAPO-34, J. South China Univ. Technol. (Nat. Sci. Ed.) 29 (2001) 30–32.
[25] P.-A. Beñat, D.L.T. Unai, J.I.-G. María, B.-L. Agustín, R.G.-V. Juan, Role of the different copper species on the activity of Cu/zeolite catalysts for SCR of NOx with NH_3, Appl. Catal. B 147 (2014) 420–428.
[26] J. Xue, X. Wang, G. Qi, J. Wang, M. Shen, W. Li, Characterization of copper species over Cu/SAPO-34 in selective catalytic reduction of NOx with ammonia: relationships between active Cu sites and de-NOx performance at low temperature, J. Catal. 297 (2013) 56–64.
[27] L. Wang, W. Li, G. Qi, D. Weng, Location and nature of Cu species in Cu/SAPO-34 for selective catalytic reduction of NO with NH_3, J. Catal. 289 (2012) 21–29.
[28] J. Wang, Y. Huang, T. Yu, S. Zhu, M. Shen, W. Li, J. Wang, The migration of Cu species over Cu–SAPO-34 and its effect on NH_3 oxidation at high temperature, Catal. Sci. Technol. 4 (2014) 3004.
[29] C.E. White, J.L. Provis, G.J. Kearley, D.P. Riley, J.S. van Deventer, Density functional modelling of silicate and aluminosilicate dimerisation solution chemistry, Dalton Trans. 40 (2011) 1348–1355.
[30] S. Fan, J. Xue, T. Yu, D. Fan, T. Hao, M. Shen, W. Li, The effect of synthesis methods on Cu species and active sites over Cu/SAPO-34 for NH_3-SCR reaction, Catal. Sci. Technol. 3 (2013) 2357–2364.
[31] L. Wang, J.R. Gaudet, W. Li, D. Weng, Migration of Cu species in Cu/SAPO-34 during hydrothermal aging, J. Catal. 306 (2013) 68–77.
[32] Y. Wan, J. Ma, Z. Wang, W. Zhou, S. Kaliaguine, Selective catalytic reduction of NO over Cu–Al–MCM-41, J. Catal. 227 (2004) 242–252.
[33] M.F. Ribeiro, J.M. Silva, S. Brimaud, A.P. Antunes, E.R. Silva, A. Fernandes, P. Magnoux, D.M. Murphy, Improvement of toluene catalytic combustion by addition of cesium in copper exchanged zeolites, Appl. Catal. B 70 (2007) 384–392.
[34] B. Chen, R. Xu, R. Zhang, N. Liu, Economical way to synthesize SSZ-13 with abundant ion-exchanged Cu^+ for an extraordinary performance in selective catalytic reduction (SCR) of NOx by ammonia, Environ. Sci. Technol. 48 (2014) 13909–13916.
[35] M. Zamadics, X. Chen, L. Kevan, Study of copper(II) location and adsorbate interaction in CuH–SAPO-34 molecular sieve by electron spin resonance and electron spin echo modulation spectroscopies, J. Phys. Chem. 96 (1992) 2652–2657.
[36] U. Deka, I. Lezcano-Gonzalez, B.M. Weckhuysen, A.M. Beale, Local environment and nature of Cu active sites in zeolite-based catalysts for the selective catalytic reduction of NOx, ACS Catal. 3 (2013) 413–427.
[37] F. Gao, E.D. Walter, E.M. Karp, J. Luo, R.G. Tonkyn, J.H. Kwak, J. Szanyi, C.H.F. Peden, Structure–activity relationships in NH_3-SCR over Cu–SSZ-13 as probed by reaction kinetics and EPR studies, J. Catal. 300 (2013) 20–29.
[38] L. Ma, Y. Cheng, G. Cavataio, R.W. McCabe, L. Fu, J. Li, Characterization of commercial Cu–SSZ-13 and Cu–SAPO-34 catalysts with hydrothermal treatment for NH_3-SCR of NOx in diesel exhaust, Chem. Eng. J. 225 (2013) 323–330.
[39] K. Leistner, L. Olsson, Deactivation of Cu/SAPO-34 during low-temperature NH_3-SCR, Appl. Catal. B 165 (2015) 192–199.
[40] Y. Cao, L. Lan, X. Feng, Z. Yang, S. Zou, H. Xu, Z. Li, M. Gong, Y. Chen, Cerium promotion on the hydrocarbon resistance of a Cu–SAPO-34 NH_3-SCR monolith catalyst, Catal. Sci. Technol. 5 (2015) 4511–4521.
[41] Y. Cao, S. Zou, L. Lan, Z. Yang, H. Xu, T. Lin, M. Gong, Y. Chen, Promotional effect of Ce on Cu–SAPO-34 monolith catalyst for selective catalytic reduction of NOx with ammonia, J. Mol. Catal. A 398 (2015) 304–311.
[42] J. Wang, Z. Peng, Y. Chen, W. Bao, L. Chang, G. Feng, In-situ hydrothermal synthesis of Cu–SSZ-13/cordierite for the catalytic removal of NOx from diesel vehicles by NH_3, Chem. Eng. J. 263 (2015) 9–19.
[43] J.C. Wang, Y. Chen, L. Tang, W.R. Bao, L.P. Chang, L.N. Han, One-step hydrothermal synthesis of Cu–SAPO-34/cordierite and its catalytic performance on NOx removal from diesel vehicles, Trans. Nonferrous Met. Soc. 23 (2013) 3330–3336.
[44] L. Pang, C. Fan, L. Shao, K. Song, J. Yi, X. Cai, J. Wang, M. Kang, T. Li, The Ce doping Cu/ZSM-5 as a new superior catalyst to remove NO from diesel engine exhaust, Chem. Eng. J. 253 (2014) 394–401.
[45] T. Yu, D. Fan, T. Hao, J. Wang, M. Shen, W. Li, The effect of various templates on the NH_3-SCR activities over Cu/SAPO-34 catalysts, Chem. Eng. J. 243 (2014) 159–168.
[46] T. Yu, J. Wang, M. Shen, J. Wang, W. Li, The influence of CO_2 and H_2O on selective catalytic reduction of NO by NH_3 over Cu/SAPO-34 catalyst, Chem. Eng. J. 264 (2015) 845–855.
[47] J. Wang, T. Yu, X. Wang, G. Qi, J. Xue, M. Shen, W. Li, The influence of silicon on the catalytic properties of Cu/SAPO-34 for NOx reduction by ammonia-SCR, Appl. Catal. B 127 (2012) 137–147.